Estimating moisture contents in the vadose zone using cross-borehole ground penetrating radar: A study of accuracy and repeatability

David Alumbaugh and Ping Yu Chang
Geological Engineering Program, University of Wisconsin-Madison, Madison, Wisconsin, USA

Lee Paprocki,[1,2] James R. Brainard, Robert J. Glass, and Christopher A. Rautman
Sandia National Laboratories, Albuquerque, New Mexico, USA

Received 29 June 2001; revised 7 May 2002; accepted 7 May 2002; published 20 December 2002.

[1] Experiments have been conducted to demonstrate the accuracy and precision of moisture content estimates derived from cross-borehole ground penetrating radar (XBGPR) measurements made within the vadose zone. Both numerical simulations and field data demonstrate that although a certain amount of image smearing occurs under ideal conditions the general trends in the spatial variation of the moisture content can be estimated by a simple empirical transformation from images of electromagnetic (EM) wave velocity. The field results are verified by comparing the radar-derived images of volumetric moisture content to neutron log derived values. When an appropriate site-specific conversion from radar wave velocity to moisture content is applied, a root mean square (RMS) error of 2.0–3.1% volumetric moisture content exists between the two sets. Further comparison of the two different data sets along with analysis of plots of the ray density through each cell indicates that regions of high moisture content are better resolved than regions of low moisture and that most of the discrepancy between radar-derived and neutron-derived moisture contents occurs in regions of high moisture content. Better spatial resolution can be provided if dense station spacing is used. However, the amount of extra time required to acquire the extra data may limit the usefulness of the method. Repeatability measurements made with five data sets demonstrate that the precision error of the data acquisition system employed averages about 0.54 ns, which translates to about a 0.5% error in moisture content estimation. *INDEX TERMS:* 1866 Hydrology: Soil moisture; 1875 Hydrology: Unsaturated zone; 1894 Hydrology: Instruments and techniques; *KEYWORDS:* GPR, vadose zone, moisture content

Citation: Alumbaugh, D., P. Y. Chang, L. Paprocki, J. R. Brainard, R. J. Glass, and C. A. Rautman, Estimating moisture contents in the vadose zone using cross-borehole ground penetrating radar: A study of accuracy and repeatability, *Water Resour. Res.*, *38*(12), 1309, doi:10.1029/2001WR000754, 2002.

1. Introduction

[2] Recent interest in vadose zone hydrology has resulted from the fact that most contaminants are released in unsaturated near-surface deposits and then transported to the underlying aquifer (saturated zone). At many contaminated sites, the vadose zone, as well as the underlying saturated region, consists of heterogeneous sedimentary deposits exhibiting a wide range of textures and depositional structures. In addition, vadose zone deposits show both spatial and temporal variability in saturation, which markedly affects flow and transport processes. Because of this, additional hydraulic information is required to characterize vadose zone flow and transport processes when compared to saturated formations.

[3] As is the case for saturated flow, the hydraulic conductivity relates the potential gradient to a flux, and accounts for resistance to flow that results from both fluid and formation properties. A decrease in saturation results in decreasing hydraulic conductivity. This, coupled with the fact that capillary tension and pore size determine the moisture content distribution within a heterogeneous formation, leads to very complex flow processes. For example, fine sediments deposited over coarse deposits may form capillary barriers to downward water flow. This can result in a saturated fine layer of clay or silt overlying a very dry layer of coarse sand. Under certain conditions this same geometry may produce wetting-front instabilities leading to preferential flow paths.

[4] The implication is that in order to characterize flow within the vadose zone, an in-depth knowledge is required of the moisture content distribution, capillary tension, unsaturated hydraulic conductivity, and the nature of spatial

[1] Formerly at New Mexico Institute of Mining and Technology, Socorro, New Mexico, USA.
[2] Now at Komex, Westminster, California, USA.

0043-1397/02/2001WR000754$09.00

variability within subsurface deposits. Because unsaturated hydraulic conductivity is dependent on saturation, and because under steady state conditions the degree of saturation may provide information on spatial variability of hydraulic properties, accurate measurement of the moisture content distribution could provide valuable information on pertinent hydraulic parameters. Additionally, detailed information on changes in moisture content over time could provide insights into vadose zone flow processes as well as provide data for predictive modeling.

[5] Traditionally, moisture content data has been obtained from field sampling, with instruments that provide sparse point measurements, or from downhole logging. Although some downhole logging techniques provide high-resolution measurements along the length of the borehole, information between boreholes can only be estimated through geostatistical or other interpolation techniques. This lack of information between sampling points and boreholes will cause uncertainties in any standard hydrologic characterization effort. Because geophysical measurements are sensitive to the physical properties between the sensor locations, these techniques are increasingly being applied tomographically to provide information on subsurface saturation fields [e.g., *Wilson et al.*, 1995].

[6] Among the various geophysical techniques, cross-borehole ground penetrating radar (XBGPR) holds promise to provide accurate estimates of 2-D and 3-D moisture content fields. XBGPR is a geophysical imaging method that can provide detailed images of the electromagnetic (EM) wave velocity within geologic materials. It is the primary dependency of the EM wave velocity on water content [*Topp et al.*, 1980] that allows XBGPR measurements to be used to produce images describing the distribution of the in situ saturation conditions within the vadose zone. The ultimate goal is to use these estimates of moisture content for a variety of applications including long-term monitoring of contaminated sites, as input to hydrologic inverse models for obtaining hydraulic property parameters that govern unsaturated flow, and to enhance the understanding of flow processes through infiltration experiments.

[7] Using surface or borehole GPR to obtain in situ moisture content is a fairly new application. *Greaves et al.* [1996] and *Lesmes et al.* [1999] used surface GPR to obtain subsurface water content, while *Hubbard et al.* [1997a] used surface GPR along with conventional hydrological data to estimate saturation and permeability. *Hubbard et al.* [1997b] employed XBGPR to estimate in situ moisture contents under static conditions, whereas *Peterson et al.* [1999] estimated porosity and permeability. Finally *Hubbard et al.* [1997b], *Eppstein and Dougherty* [1998], and *Binley et al.* [2001] used XBGPR to compare velocity changes before and after infiltration in order to image relative moisture changes. The primary discussion of accuracy and precision in any of these previous papers, however, tends to focus on the appropriate choice of a petrophysical relationship to convert the GPR results to moisture content [e.g., *Greaves et al.*, 1996; *Binley et al.*, 2001], rather than on errors associated with the data measurement and imaging processes. This paper discusses an exercise that was conducted prior to, and during, an infiltration experiment designed to investigate the physics of 3-D, transient, unsaturated flow and transport processes within the vadose zone. Here we examine the usefulness of the XBGPR imaging method for establishing in situ estimates of moisture content, and to illustrate errors in these estimates that are associated with the physics of the method, data acquisition, and processing. The study presented here can be thought of as a more specialized companion paper to the work presented by *Peterson* [2001], who described the basics of the XBGPR tomography method, and documents certain errors that can occur during data collection that need special attention during processing.

[8] After a description of the data acquisition system and processing that is applied, a general explanation of the assumptions that are made to process the XBGPR data is provided. This is followed by demonstrations of how these assumptions in processing can lead to accuracy errors within the resulting estimates of in situ moisture content. These demonstrations involve both numerical examples as well as field tests to show how assumptions that are made effect the images, how the region between the boreholes is sampled by the EM wave field, and how the data sampling density affects image resolution. These accuracy demonstrations are followed by an analysis where repeatability measurements are used to assess measurement precision.

2. XBGPR Data Acquisition and Processing Techniques

[9] In this study the Sensors and Software PulseEKKO 100 GPR system was employed in the cross-borehole configuration. When employed in this manner an electric dipole antenna in one borehole transmits a pulse, while a second antenna positioned in a second borehole located a few meters away measures the direct and scattered EM wave field. For a given source–receiver pair, the datum of interest is the travel time of the direct wave from the source to the receiver, which yields an estimate of the EM wave velocity of the material between the two antennas. Measurements of the travel time for multiple source and receiver pairs allows the 2-D velocity structure between the boreholes to be reconstructed using tomographic techniques. The reader is referred to the work of *Peterson* [2001] for a more in-depth discussion of the processing required for the XBGPR imaging method.

[10] Unless noted otherwise, the data collection parameters included using a center frequency of 100 MHz along with a 0.25 m incremental-depth-sampling interval for both the transmitter and the receiver. This sampling interval was chosen for two reasons. First, it is the suggested interval provided by the manufacturer in order to avoid problems with spatial aliasing or undersampling. Second, this sampling interval required 6 hours of acquisition time to collect a full round of data at the site described below. Halving the sample rate to 0.125 m in order to increase resolution would have quadrupled the number of data, as well as the time required for the acquisition of each data set. Thus decreasing the sample interval would produce an excessive burden when multiple data sets are collected in order to monitor the transient infiltration event.

[11] To ensure accurate data in the presence of instrument drift, calibration files were collected after every tenth transmitter position. As described by *Peterson* [2001], this involves collecting a series of traces with both the source and receiver at a known separation in a medium of known

velocity, i.e., in the air, and from these results determining a ''time-zero'' correction to be applied to all subsequent data. Although the multiple calibration files causes added complexity when processing the data, it was found to produce better images, especially in those cases when the XBGPR antennas were near the bottom of the boreholes.

[12] Experiments conducted during site construction showed that subsurface cables installed for communication with other hydrological and geophysical instruments influenced the XBGPR measurements when the acquisition angle (the angle formed between a line drawn from the source to the receiver, and a line parallel to the Earth's surface extending outward from the source toward the receiver well) exceeded 45°. It is postulated that the cables provide a waveguide such that the quickest path from the source to receiver for large-aperture measurements is not through the ground, but rather is due to reradiated energy from the cable(s). *Peterson* [2001] observes similar problems in XBGPR data he analyzed when the angle exceeded 50°. Thus to avoid problems with this phenomenon, the maximum acquisition angle was restricted to 45°.

[13] The XBGPR results presented in this paper have been processed in the following manner. First, the data were calibrated for time-zero using the process discussed above. Second, the first arrival, or EM wave travel times were ''picked'' using Sensors and Software's PulseEKKO 100 data processing package. Third, the travel time data were inverted using a scheme published by *Aldridge and Oldenburg* [1993] to produce a 2-D image of EM wave velocity. This scheme was originally designed for inverting seismic travel time data and employs least squares inversion methodology along with ''smoothness'' constraints to produce a smoothed estimate of the velocity. The constraints are applied by minimizing the velocity gradient between adjacent cells within the image domain in both the horizontal and vertical directions. The tomography code uses a finite difference travel time computation of *Vidale* [1988] to compute curved-ray travel times between the source and receiver. After the data inversion process has been completed, the velocity image is converted to an image of the dielectric constant, and finally to moisture content using an empirical relationship between the EM velocity and the water content.

[14] When converting GPR velocities to dielectric constant it is usually assumed that the magnetic permeability is that of free space and that the electrical conductivity is relatively low, say less than 0.03 S/m. Under these assumptions the conversion from EM wave velocity to dielectric constant is given by the expression

$$\varepsilon = (c/v)^2 \tag{1}$$

where ε is the dielectric constant (dimensionless), c is the velocity of light in a vacuum ($\varepsilon = 1$), and v is the EM wave velocity of the medium as determined from the measurements [*Reynolds*, 1998]. After this simple conversion from velocity is completed, the dielectric values are converted to moisture content via an additional empirical relationship (the relationship employed is discussed in more detail below). In most cases, moisture content is directly proportional to the dielectric constant, and therefore inversely proportional to the velocity.

[15] Each one of the steps above may introduce different levels of accuracy error into the final interpretation. First of all there is the error introduced via the data acquisition configuration and tomographic imaging algorithms that are employed. As demonstrated by *Kak and Slaney* [1988], in order to exactly recover an image of the region of interest, the arrival time data must be acquired in a fashion that completely surrounds the region. In addition, the data must be sampled spatially at an interval that is finer than the smallest scale inhomogeneity to be resolved. Unfortunately logistical constraints usually do not allow for the former, while acquisition time constraints limit the spatial sampling density that can be achieved. Further complications exist in travel time tomography due to the fact that first arrival energy is often refracted around low-velocity zones, and therefore these regions will be poorly sampled.

[16] All of these limitations result in lower resolution within the images, as well as the introduction of nonuniqueness, inaccuracy, and instability into the data inversion process. To overcome the latter two problems, constraints such as those employed by *Aldridge and Oldenburg* [1993] can be incorporated. However, this introduces another assumption as now the image is forced to be smoothly varying across the section, which may violate the true geology thus leading to additional accuracy errors.

[17] Next there is the conversion from velocity to dielectric constant, which employs (1), and then an empirical conversion from dielectric constant to moisture content. Both of these conversions can provide large sources of accuracy error if the underlying assumptions are not valid. Finally, there is the issue of measurement system precision, and how that error influences the final results. Although this type of error can be overcome by collecting multiple data sets and then averaging the results, the acquisition time required for this process may not be allowed given the nature of the transient conditions in moisture that we ultimately hope to image. Thus the level of precision error must be investigated. We address these types of errors below, state how we partially accounted for them, and also discuss the inaccuracies that still remain after the corrections have been applied.

3. Image Processing Accuracy in Determining Velocity

[18] A numerical example has been constructed in order to investigate the accuracy of the velocity image that is recovered from the XBGPR data under ideal conditions. Here, ''ideal'' implies noise-free data generated from a model of known EM properties. The EM parameters and borehole separations incorporated into the model are representative of those found at the field site.

[19] The known model is shown in Figure 1a. Areas of low velocity (high electrical conductivity σ and dielectric ε) located toward the top and middle of the model represent regions of high moisture content associated with fine textured deposits, which, because of small pore size, have a high moisture retention capability. The low-velocity region at the bottom of the image represents the saturated zone. Although the water table was not encountered at the experimental site described below, this was included here to provide a zone of minimum velocity. The higher velocity areas, then, represent regions of low moisture content associated with coarse textured deposits of low moisture retention capability.

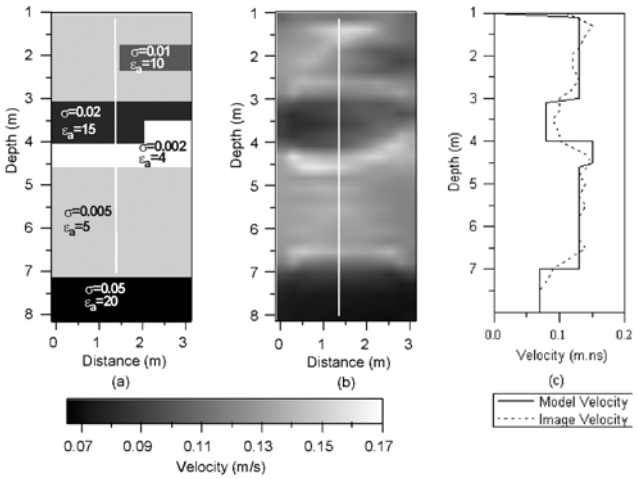

Figure 1. (a) Model of EM properties employed in the numerical simulation. (b) Image resulting from tomographic reconstruction of a synthetic data set that was calculated from the model in (a) as described in the text. (c) Vertical profile of velocity along the white lines shown in (a) and (b).

[20] The synthetic EM results for this model were computed using the 3-D, full wave-equation modeling scheme of *Wang and Tripp* [1997]. This scheme employs a finite difference time stepping algorithm to determine the vector EM field at any point in space and time produced by an electric-dipole source. Thus the output will be a series of amplitude-versus-time traces for each source–receiver pair, similar to those acquired in the field. The XBGPR simulation was configured with a source and receiver sampling interval of 0.25 m in, and a separation of 3 m between, the two vertical boreholes. The first arrival times were determined from the synthetic data and then input into the inversion scheme. Note that in this model, we have not included the air–Earth interface. Initial trials indicated, for the sensor configuration employed here, numerical errors were introduced into the results calculated with the *Wang and Tripp* [1997] scheme when this boundary between low and high velocity zones was included in the model. The effect of this interface on the velocity estimates will thus not be addressed with this numerical example.

[21] The velocity image that results from the inversion portion of the processing is shown in Figure 1b; a comparison of the model and the image along a vertical profile is included in Figure 1c. Notice that a smoothly varying model is recovered which maintains the general trends of the known structure, and therefore we have met our primary objective. However, significant smearing occurs across boundaries in the image, and this smearing appears to be worse at the center of the image than near the boreholes. Also notice that "oscillations" occur between low and high the velocity zones; this is especially apparent in Figure 1c. For example, although the model transitions directly from the high to the low velocity zone at a depth of 7 m, the velocity image first increases before decreasing as a function of depth. Both of these phenomena can be attributed to the smoothness constraints imposed within the inversion scheme as well as to limitations imposed by the tomographic imaging geometry. Also, the smearing not only has the effect of reducing the image resolution but also causes the true velocity within some regions to be overestimated or underestimated. Examples of this phenomenon can be found within the low-velocity zone at 2 m depth, and within the high-velocity zone toward the center of the image, respectively. Overall, the root mean square (RMS) error between the image and the known velocity model is 0.015 m/ns.

[22] The above example illustrates how well we can recover the model under perfect conditions. However, when analyzing field data, the true model is unknown and thus it is difficult to assess the level of accuracy directly from the image. Although methods exist for assessing image uncertainty through the analysis of parameters such as the model covariance matrix as proposed by *Tarantola* [1987], these can be computationally demanding. Here, we will employ less rigorous methods of estimating the accuracy of the image domain by examining the "ray density" through each cell. The ray density method is a modification of the standard ray coverage diagram [e.g., *Bregman et al.*, 1989; *Aldridge and Oldenburg*, 1993], that has traditionally been employed to analyze cross-borehole seismic travel time images, and is calculated by taking the total length of all the rays passing through a specific cell and then normalizing by the cell size. Thus, the values of ray density are dimensionless. Because the ray paths describing the EM wave first arrivals represent the fastest path between the transmitter and receiver, the rays tend to refract around areas of low velocity or high moisture content and are concentrated in regions of high velocity or low moisture content. Therefore, to at least a first order, the ray density image should reflect the travel time image shown in Figure 1b.

[23] The first-arrival ray density corresponding to the image in Figure 1b has been plotted in Figure 2; note that we have employed a reversed gray scale scheme in this case. Low ray density regions are found at depths of 2, 4, and below 7 m depth where low-velocity regions are imaged. Also notice the areas of high ray density surrounding these lower values; these regions correspond to the highest velocities within the image (Figure 1b). Although the conclusions derived in this manner are relative, we can deduce from these results that high-velocity areas are better resolved than the low-velocity regions, especially for those regions just outside the low-velocity zones. In addition, those cells in the center of the low-velocity regions have almost no rays passing through them, and thus the imaged velocities are suspect. Finally, the fact that the first arriving energy takes a path around the low-velocity zones highlights the need for using tomography algorithms that incorporate curved ray paths, as not incorporating this into the analysis may lead to image artifacts in those locations where large velocity contrasts are present.

4. Experimental Site Description

[24] To test the applicability of XBGPR data for recovering the in situ moisture content distribution within the vadose zone, measurements were made at a hydrologic/geophysical vadose zone field site in Socorro, NM. The experimental site was developed as part of an ongoing experiment to describe unsaturated flow and contaminant transport within the vadose zone [*Brainard et al.*, 2002], as well as to provide input parameters for a geophysical/hydrologic inverse scheme [*Hughson and Yeh*, 1998].

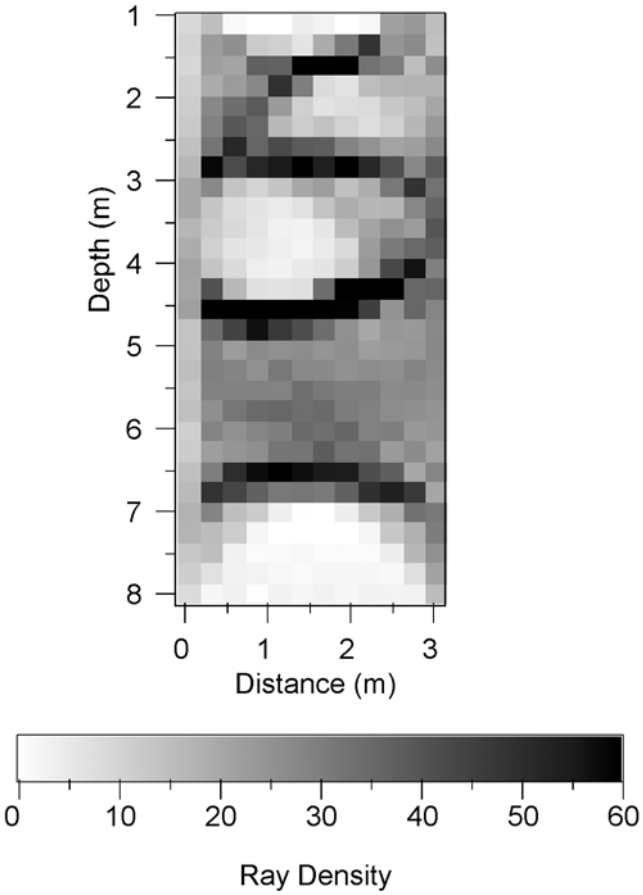

Figure 2. Ray path density across the image region for the image shown in Figure 1b. The ray path density is defined as the total length of rays through a given cell divided by the length of the cell.

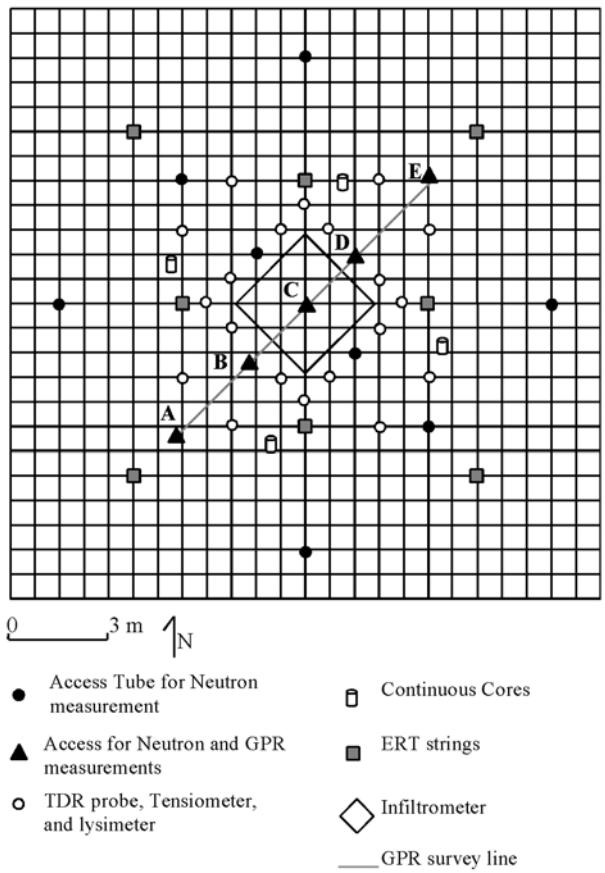

Figure 3. Plan view showing the locations of the hydrologic instruments and boreholes used for neutron and XBGPR measurements.

[25] The sediments at the field site are mapped as part of the Sierra Ladrones Formation of the Upper Santa Fe Group. Locally the formation consists of unconsolidated and heterogeneous interbedded sands, gravels, and clay, all associated with the ancestral Rio Grande fluvial system [*Hawley*, 1983]. Cuttings from 41 instrumentation boreholes and 4 continuous core samples detailed in Figure 3 provided the basis for a 3-D model of the deposits within the instrumented volume. Simplified stratigraphic columns constructed from the 4 continuous core samples are shown in Figure 4 to depict spatial relationships of the continuous core sample locations, mappable geologic units, and the transect consisting of 5 PVC case boreholes used in the XBGPR study presented in this paper. EM induction and natural gamma borehole logging aided in locating and verifying contacts between units of contrasting conductivity and mineralogy [*Brainard et al.*, 2002], and exposures in trenches and a nearby sand quarry provided the opportunity to gain additional geologic information through direct observation.

[26] The dimensions of the instrumented site are 10 m on a side with PVC-cased subsurface access tubes installed to a maximum depth of 13 m (Figure 3). XBGPR data were collected along the SW-NE diagonal, which includes four transects between 5 PVC-cased boreholes. The XBGPR data collection was limited to the SW-NE diagonal due to the previously described possibility of interference from

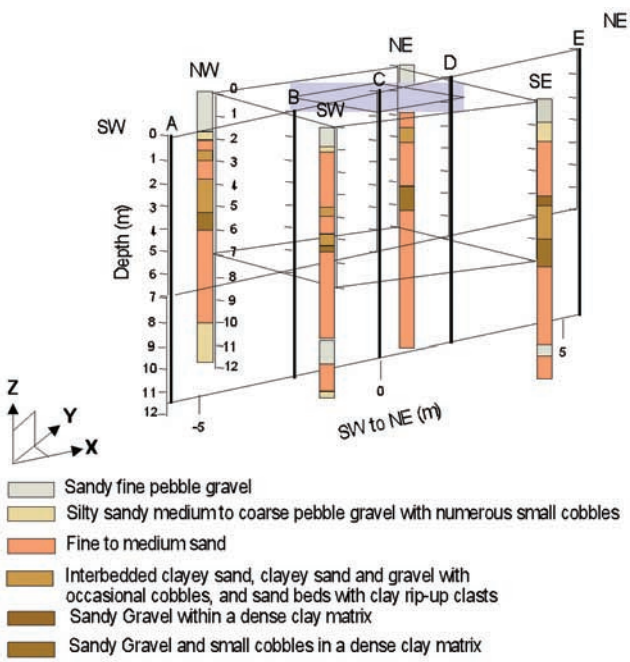

Figure 4. Four stratigraphic columns that were constructed from continuous core collected in the designated boreholes shown in Figure 1.

electrical cables permanently installed for electrical resistivity tomography (ERT) measurements and various other hydrological instruments. To minimize these effects, the cables were routed away from this profile during site construction.

[27] This paper contains an analysis of five data sets collected over a 4-month period starting in November 1998 and extending into February 1999, which were collected prior to starting the infiltration experiment, and one spatially dense data set that was collected approximately 1 year after infiltration was initiated. Neutron probe measurements were acquired in conjunction with the XBGPR and other geophysical measurements to recover in situ moisture contents immediately surrounding the PVC-cased boreholes shown in Figure 3. Although the XBGPR and neutron measurements inherently sample different volumes of material, calibrated neutron logs provide an efficient method of estimating moisture contents along the borehole, and therefore provide an effective check on the GPR-derived values. In order to best compare these two sets of estimates, neutron measurements were also collected with a 0.25 m sampling interval. The calibration of the neutron probe "counts" to moisture content was accomplished using an experimentally derived expression developed by correlating neutron counts to time domain reflectometry (TDR) measurements of moisture contents in deposits at the site [*Paprocki*, 2000].

5. Velocity Imaging of Site Data

[28] The image processing steps outlined in section 3 have been applied to one of the five preinfiltration data sets collected at the site, the results of which are presented in Figure 5. Here, the vertical white lines represent the locations of the wells. First, notice that there exists a fair amount of spatial variability in the imaged velocities (Figure 5a). Also, as expected, the resulting image is smooth in nature as we would expect from the aforementioned discussion on the imaging methods employed.

[29] The primary issue to investigate is how well the image reproduces the known stratigraphy. In unsaturated porous media under steady state conditions, clay and silt exhibit higher moisture retention capabilities than gravel or sand due to the smaller pore size. Because in most cases moisture content is directly proportional to dielectric constant which is inversely related to the velocity, the velocity in turn is inversely proportional to the moisture content. Therefore high-velocity zones should correlate to sand and gravel layers, while low-velocity regions should correlate to clay and silt layers. Based on the above information and comparing the image in Figure 5a to the SW and NE stratigraphic columns shown in Figure 2, it appears that geological textures can be identified within the velocity images. That is, the clay units depicted in the stratigraphic columns correspond in-depth to the low-velocity zones of the XBGPR images, while the sands and gravel correlate with higher-velocity regions. In addition, variations that appear in the stratigraphic columns also appear to be present within the image. For example, both the stratigraphic columns and the GPR image show that one layer of low-velocity material bearing fines exists to the NE between 4 and 6 m, whereas two exist to the SW with an intervening "tongue" of coarse material. Therefore, the imaging results given in Figure 5a indicate that the XBGPR images can not only nondestructively provide realistic images of the spatial variability within the subsurface, but that the resulting images agree with the known geology.

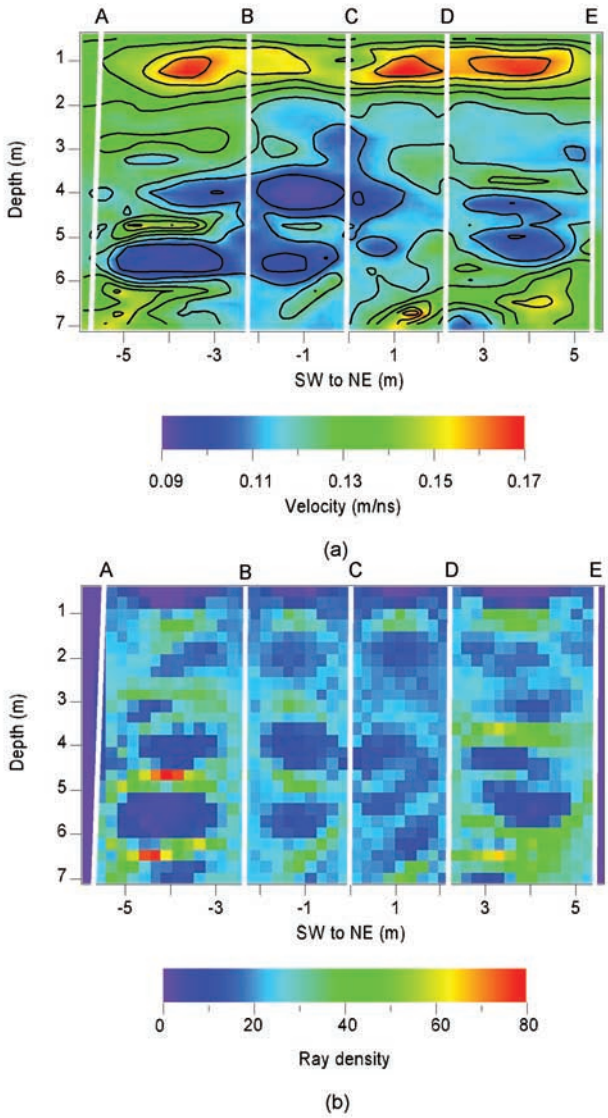

Figure 5. (a) The velocity image created from one of the five preinfiltration XBGPR data sets collected at the Socorro vadose zone test site. The vertical white bars represent the location of the PVC-cased boreholes. (b) Ray density across the image region. The ray density is defined as the total length of rays through a given cell divided by the length of the cell.

[30] Figure 5b details the ray density across the image region. As noted in Figure 2, the ray density is small within the low-velocity zones and greater within surrounding regions. Maybe more importantly, very few ray paths intersect cells located within the upper meter. Due to the higher velocity of the air relative to the ground, ray paths corresponding to the first EM wave arrival for sources and receivers near the surface refract along the Earth–air interface rather than travel through the ground. Because few rays traverse the material between these near-surface sensors, the EM velocity field in the sediments within the upper meter is poorly resolved.

[31] One issue that has not been determined by any of the above analysis is how different data acquisition strategies affect the spatial resolution of the image. To resolve one aspect of this issue, a high-density data set was collected in the spring of 2000 after 1 year of infiltration. These data were acquired using a 200 MHz center frequency and a sampling interval of 0.125 m. This "high-density" data set was then decomposed to produce a second data set that employs a 0.25 m sampling interval, such that the only difference between the two is the data density. The two different data sets were then inverted, each using a cell size equal to the data sampling interval. It is evident from the results shown in Figure 6 that the higher density yields greater spatial resolution, i.e., finer details appear in the image. Thus a certain level of error is incurred simply by not sampling the data at a fine enough level. However, as alluded to before, finer sampling means a greater amount of time to acquire the data. In this case it took approximately four times longer to collect the 0.125 m data than the 0.25 m case, which made it infeasible to routinely acquire high-density data during the infiltration experiment. Thus image resolution had to be sacrificed in the essence of a reasonable acquisition time.

6. Accuracy Issues in Converting Velocity to Moisture Content

[32] The expression given by (1) is normally employed to convert velocities to dielectric constant, which is in turn converted to an image of moisture content. The conversion to moisture content often employs Topp's equation [*Topp et al.*, 1980] which is given as

$$\theta = -5.3 \times 10^{-2} + 2.9 \times 10^{-2}\varepsilon - 5.5 \times 10^{-4}\varepsilon^2 + 4.3 \times 10^{-6}\varepsilon^3. \quad (2)$$

This empirical expression was derived for converting TDR measurements of soil-dielectric constant to estimates of volumetric moisture content, and involved laboratory measurements for a wide variety of sand and clay samples. Because the XBGPR and TDR methods obey the same physics and measure the same physical property, i.e., EM wave velocity, the Topp equation can be applied in both cases.

[33] At the Socorro site, Topp's equation was found to overestimate the moisture content. This is not an uncommon occurrence as problems associated with using Topp's equation for estimating moisture contents can be found throughout the GPR and TDR literature. For example, *Binley et al.* [2001] theoretically compare moisture contents derived by Topp's equation to those derived with the Complex Refractive Index Method (CRIM) presented by *Chan and Knight* [1999] to demonstrate how high dielectric constants of the matrix material will yield poor estimates of moisture content if the former is employed as the petrophysical conversion. *Dirksen and Dasberg* [1993], *Jacobsen and Schjønning* [1993a, 1993b], and *Zegelin et al.* [1992] all discuss problems with using Topp's equation to convert TDR-derived dielectric constants to moisture content in regions of higher than normal soil conductivity caused by the presence of clay, saline fluids, and/or the presence of organic matter. *Robinson et al.* [1994] discuss similar problems when magnetic minerals are found in the soil. The presence of these minerals increases the bulk magnetic permeability of the soil, which provides for lower EM wave velocities. This is likely a major part of the problem associated with using (2) at the STVZ site as approximately 5% magnetite by weight was found in the near-surface sands.

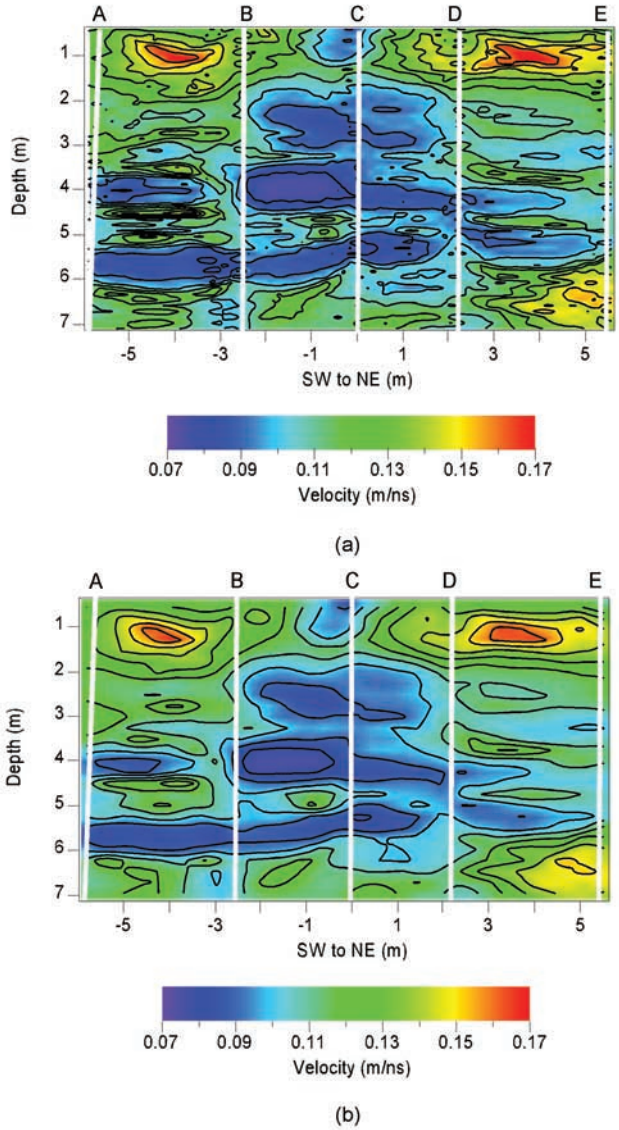

Figure 6. (a) The velocity image created from a postinfiltration XBGPR data sets collected at the Socorro vadose zone test site using a 200 MHz antenna with a 0.125 m downhole sampling interval. The vertical white bars represent the location of the PVC-cased boreholes. (b) The velocity image created from postinfiltration XBGPR data sets collected at the Socorro vadose zone test site using a 200 MHz antenna with a 0.25 m downhole sampling interval. The vertical white bars represent the location of the PVC-cased boreholes.

[34] To more accurately estimate moisture contents from the GPR velocity images, a site-specific conversion was developed by incorporating TDR measurements of dielectric constant derived from (1) versus moisture content made on samples collected on site. In Figure 7 the dielectric constant derived from one set of TDR measurements is plotted against laboratory measured moisture contents. For

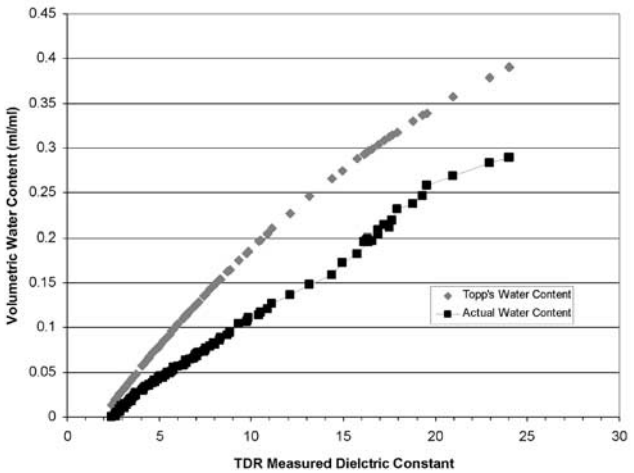

Figure 7. TDR-measured apparent dielectric constant versus actual moisture content and that estimated using Topp's equation [*Topp et al.*, 1980] for a soil sample collected at the Socorro infiltration site.

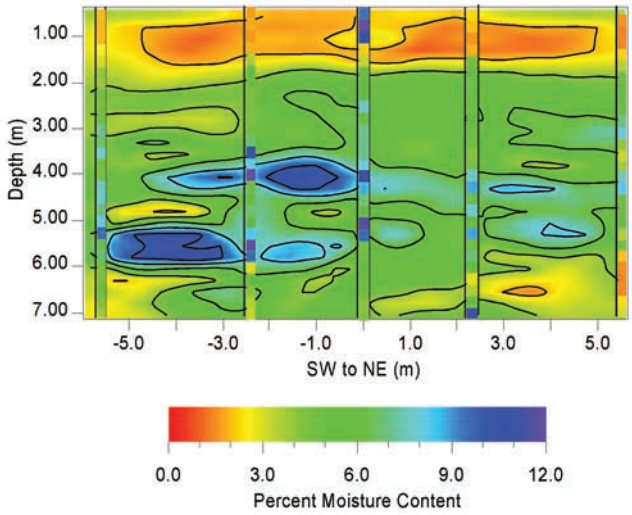

Figure 8. The moisture content image created by applying the conversion given in (3) to the velocity image shown in Figure 5a. The vertical bars of color represent calibrated neutron data collected within the wells.

comparison the moisture content predicted by Topp's equation [*Topp et al.*, 1980] has also been included. The sand employed in this study was collected from the top meter at the experimental site. The data were collected as part of a TDR calibration process similar to that described by *Young et al* [1997]; more complete details are given by *Paprocki* [2000]. As Figure 7 demonstrates, Topp's equation markedly overestimates the moisture content within the sample.

[35] To develop the site-specific expression, a linear regression was applied between the measured dielectric constant and water content values for a combined data set consisting of the TDR measurements shown in Figure 7, plus two other sets of measurements made with different probes. Because the combined set of measurements exhibited more scatter than the single result shown in Figure 7, a linear rather than higher order regression was employed. The resulting relationship has the form

$$\theta = 0.0136 * \varepsilon - 0.033. \quad (3)$$

It must be noted that converting to moisture content using this process has associated with it a different set of errors, most of which have to do with the assumption that one calibration is valid for all the materials at the site. In reality, because the materials vary across the site, and thus the electrical conductivity and/or magnetic permeability differs from one location to the next, the conversion also likely varies in both the vertical and horizontal directions. However, providing a calibration for all of the different materials found at the site would be an extensively time consuming process, and thus only the expression given by (3) has been applied to date.

[36] The image of moisture content that results from converting the XBGPR velocity image is given in Figure 8; the vertical bars of color at the well locations represent the neutron log derived moisture contents in each of the wells. A more direct comparison between the XBGPR and neutron results in each borehole is given in Figure 9.

Figures 10 and 11 present similar comparisons of neutron-derived and XBGPR-derived moisture contents for the velocity images in Figure 6. Overall, the XBGPR and neutron measurements match fairly well, with a RMS discrepancy of 2.0% volumetric moisture content for Figure 8, and 3.1 and 2.2 for Figures 10a and 10b, respectively. (These RMS values correspond to depths greater than 1 m, as the results tend not to match as well above this depth due to the aforementioned problems in near-surface XBGPR imaging.). Both methods measure high moisture contents between 4 and 6 m depths, and both record low moisture contents between 0 and 2 m depths away from the infiltrometer. Given the results of the numerical studies presented earlier, it is not surprising that the XBGPR images reconstructed using the data collected with a 0.25 m sampling interval (Figures 8 and 10b) are smoothed versions of the neutron logs. However, notice in Figures 10 and 11 that the data sampled at 0.125 m appear to be able to recover more spatial variability when compared to images

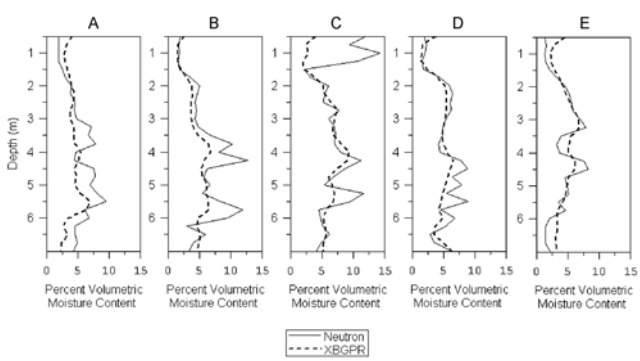

Figure 9. Comparison of the neutron-derived and XBGPR-derived moisture content estimates within the five boreholes used to acquire the data. The Topp's and site-specific estimates have been derived from Figure 7 and this figure, respectively.

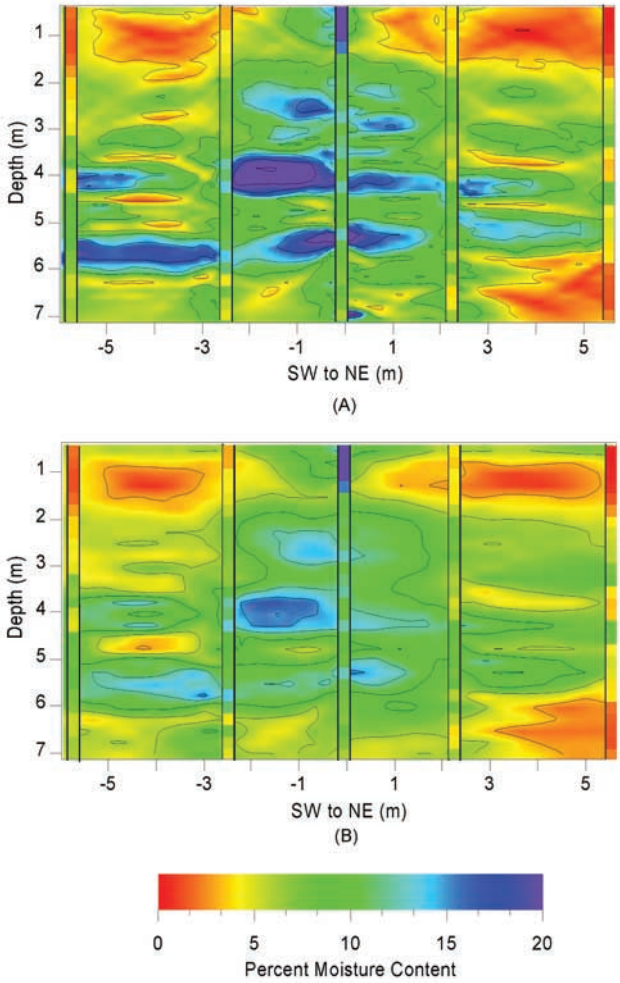

Figure 10. (a) The volumetric moisture content image resulting from the velocity image shown in Figure 6a. A data sampling interval of 0.125 m was employed. (b) The volumetric moisture content image resulting from the velocity image shown in Figure 6a. A data sampling interval of 0.25 m was employed.

reconstructed from the 0.25 m sampled data. In many cases images reconstructed from the more coarsely sampled data result in ''smoothing'' multiple highs and lows present in both the neutron data and the image produced from the denser sample interval. Figures 10 and 11 clearly illustrate how the spatial resolution can change if different data sampling is employed.

[37] Although the XBGPR images are able to recover the general trends in the moisture content, and in general provide reasonable estimates of moisture contents within the drier zones, the images do not accurately recover high moisture content values within many of the ''peaks'' present in the neutron data. This is especially true of the high data density image shown in Figure 10b. In fact, it is these peak regions in which most of the RMS error between the neutron and XBGPR estimates is accumulated. An interesting note is that the XBGPR images tend to underestimate the moisture contents within these zones in the preinfiltration images (Figure 9), while overestimating them in the postinjection images (Figure 11).

[38] At least part of these discrepancies can be attributed to the insensitivity of the XBGPR to zones of high moisture content as determined from the ray density plots (for example, Figure 5b). This is especially true for the high neutron values near surface in the center well where high moisture contents arise from a bentonite plug in the annulus around the access tube. Because the center access tube was installed in the infiltrometer, bentonite was used as a backfill between 0.3 and 0.67 m to reduce the possibility of preferential flow down the sides of the tube during infiltration. The bentonite was emplaced dry, and then water added to induce swelling and thus seal the well. The XBGPR measurements did not record this zone of high moisture content due to the limited extent of the saturated plug, and, as was discussed in section 5, because the very near-surface and is poorly resolved due to refraction of the ray paths along the surface–ground interface.

[39] A second explanation for the observed discrepancies between XBGPR-derived and neutron-derived moisture contents may be due to fact that neutron values are spatially averaged over the measurement volume surrounding the neutron source. A crude estimate of this measurement volume is a sphere with a radius of 0.5 m [*Wilson et al.*, 1995]. The neutron probe tends to ''smooth'' through high moisture content zones, which are smaller than this ''sensitivity'' radius. This smoothing results in values less than the true highest moisture content within the measurement sphere. Thus in some cases the XBGPR may actually be yielding more accurate estimates of volumetric moisture contents. However, (1) there is no way to confirm this with the data collected thus far in this experiment and (2) the discrepancies are probably arise from both the XBGPR's insensitivity to regions of high moisture content and the volumetric averaging of the neutron measurement.

[40] Finally, the XBGPR estimates of moisture content appear to be somewhat smeared along the borehole, and regions of high moisture content seem to ''pinch-out'' near the access tubes. Although this may be a problem associated with the imaging procedure, these phenomena may also at least partially result from the ability of XBGPR to image near-hole disturbances caused by the casing installation

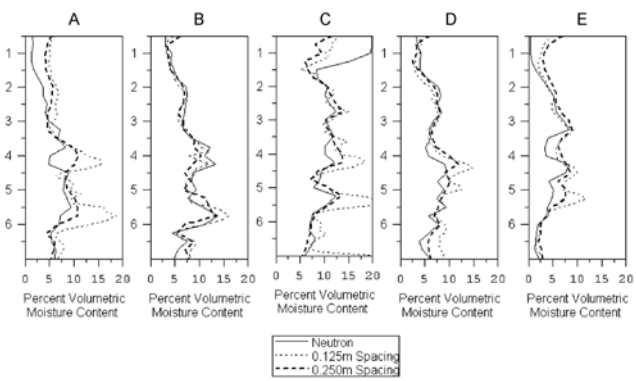

Figure 11. Comparison of the XBGPR-derived moisture content estimates within the five boreholes used to acquire the data. The comparisons are between the neutron-estimated moisture contents and those derived from the images in this figure using 0.125 and 0.25 m data sampling intervals.

procedure. The boreholes were drilled with a 6-inch diameter hollow stem auger, which inevitably left an 8-inch borehole. After the PVC casings were installed, the borehole was backfilled with dry surface sand creating both a discontinuities in the moisture content and the stratigraphy [*Brainard et al.*, 2002]. It is also likely that some drying of the subsurface sediments may have occurred between the time the hole was drilled and the time the casing was installed, as well as a result of the redistribution of moisture into the dry backfill. It is plausible that the XBGPR measurements are sensing these disruptions in the stratigraphy and moisture content, and imaging it as a discontinuity in high moisture regions across the borehole. This phenomena that would not be detectable with neutron measurements due to the relatively large measurement sphere.

7. Repeatability

[41] A repeatability analysis was accomplished using the five data sets that were collected prior to infiltration. The measurements were made after covering the experimental site with a tarp, which was then buried to a depth of 20–30 cm with sand. The primary purpose of the tarp was to exclude uncertainties associated with both evaporation and inadvertent infiltration from storms. However, prior to infiltration this likely resulted in state conditions, and therefore the variations between the five data sets will be due to XBGPR repeatability error only. Steady state conditions were verified by the lack of trends in both neutron and XBGPR data sets taken over time.

[42] The repeatability error has been calculated as the RMS difference between the travel time measurements as well as the corresponding moisture content images. Because both the errors in the original data and the resulting images are being determined, the translation of error from the raw data to the image can also be determined in a general sense. However, the interpretation of these results must be constrained with the fact that we are only using five data sets which represents a statistically small sample size.

[43] The repeatability errors were estimated by calculating the RMS error of the five different data sets against the mean value. For the data analysis, the travel times for each well pair were evaluated separately (Figures 12a–12d). The transmitter depths are plotted versus receiver depth with zero representing the ground surface. The regions in the upper left and lower right quadrants of the figure are blank (or white) due to the 45° data acquisition angle that was employed as described in a previous section. Horizontal and vertical bands of missing data are due to bad receiver or transmitter positions, respectively, in at least one of the five data sets.

[44] The RMS repeatability error for each well pair is AB −0.86 ns, BC −0.40 ns, CD −0.45 ns, and DE −0.48 ns, and the total RMS error for all four well pairs is 0.54 ns. Well pair AB has the highest error, which occurs where the transmitter is between 5.2 and 7 m depth, and the receiver is between 3 and 5 m. This large error is due to one bad data set that had significantly different travel times over these positions than the other four data sets, and is likely due to instrument instability.

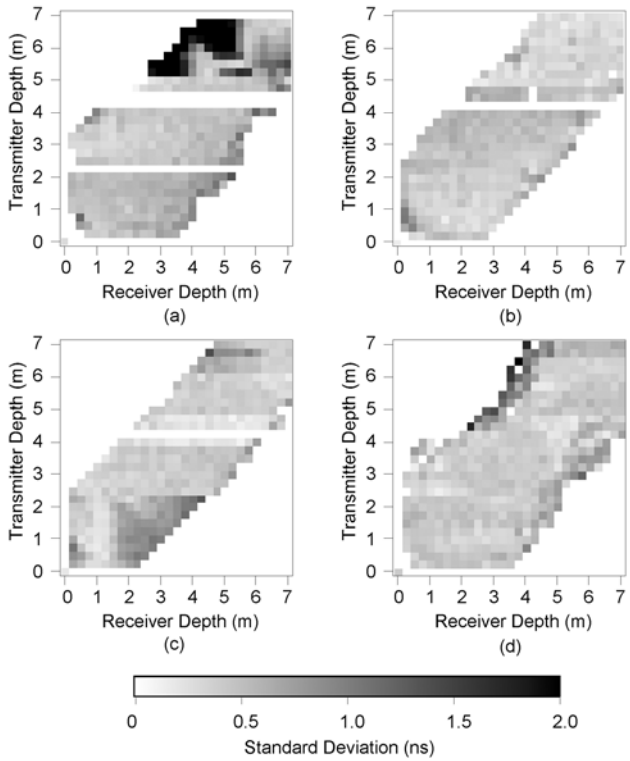

Figure 12. Standard deviations for the five travel time data sets collected between November 1998 and March 1999. (a) The AB well pair. (b) The BC well pair. (c) The CD well pair. (d) The DE well pair.

[45] Figure 13a shows the mean moisture content image resulting from averaging the moisture content images produced from the five data sets, while Figure 13b shows the RMS difference from the mean. Notice that there are only minor differences between Figures 8 and 13a. The absolute moisture content error ranges from 0% to 1.5% volumetric moisture content; however, the majority of the values are less than 1% volumetric moisture content, while the RMS repeatability error is 0.50% volumetric moisture content. The larger errors generally correlate with areas of higher moisture content. For example, the highest error (1.5%) is found at 4 m depth where the first layer exhibiting high moisture contents occurs. In addition, the error is higher in the SW around 4 and 6 m where the two high moisture content layers occur. This correlates with the ray density analysis in section 5 which indicated that regions of high moisture content will be poorly resolved compared to the dry regions. Overall this analysis indicates that for this experiment, a travel time repeatability error of 0.54 ns translates to a volumetric moisture content error of 0.50%.

8. Conclusions

[46] Our results using both synthetic data and field measurements indicate that XBGPR can be used to estimate the in situ moisture content distribution in a heterogeneous environment. With the instruments and well separations employed in this experiment, an instrument precision analysis from repeatability measurements

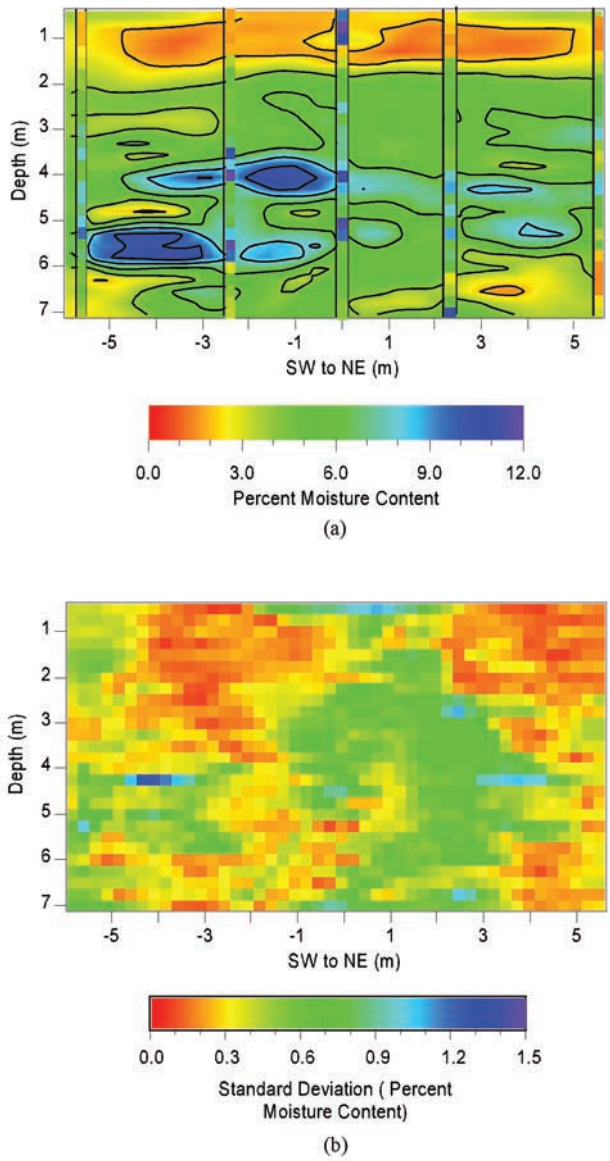

Figure 13. (a) The mean moisture content image created by averaging the five XBGPR data sets collected at the Socorro vadose zone test site between November 1998 and March 1999. The vertical bars of color represent calibrated neutron data collected within the wells. (b) Standard deviation from the mean of the five moisture content images between November 1998 and March 1999.

yields a RMS error of 0.5% volumetric moisture content, while a comparison against neutron moisture estimates yields a RMS accuracy error of 2.0–3.0% volumetric moisture content. We note however, a conversion specific to the materials found at the site was applied to provide this level of accuracy. The results also indicate that the images are a smeared version of the true distribution (at least when readily available imaging packages are employed), but that the smearing can be at least somewhat reduced by sampling the data using higher spatial densities. It has been demonstrated through the use of ray density diagrams as well as the images of moisture content themselves that regions of high moisture content will be more poorly resolved than regions of low moisture content, and that travel time data collected when both the sources and receivers are near the Earth's surface result from refraction along the air–Earth interface rather than through the subsurface materials. Thus near surface sediments will be poorly resolved when using this configuration. This analysis provides a baseline to assess the accuracy of, and uncertainty in, GPR-derived estimates of moisture content. Theoretical approaches such as that employed by T.-C. J. Yeh et al. (Uncertainties in interpretation of electrical resistivity survey in subsurface hydrological applications, submitted to *Water Resources Research*, 2001) could be applied to further refine the conclusions about uncertainty. However, there are several issues that have not been addressed in this study. The topic of subscale heterogeneity has been touched upon in the resolution study, but not fully investigated. An increase in the spatial sampling density will increase the spatial resolution to a certain degree, but at some point an optimal resolution will be achieved. The effect of heterogeneity that is at a scale finer than this optimal resolution could be a very important topic when analyzing vadose zone flow. *Chan and Knight* [1999] discuss a related problem associated with estimating moisture contents from TDR measurements if the formation exhibits anisotropy. Anisotropy can occur if the interbedding scale is smaller than the sensor spacing. Simple tests to determine if anisotropy is present at the STVZ site have proven inconclusive, thus here we have assumed an isotropic subsurface which may be inappropriate.

[47] A third topic of interest that could provide for additional error in our moisture content estimates is hysteretic effects due to wetting and drying processes. *Knight and Nur* [1983] show that at sub-GPR frequencies a hysteretic relationship is evident between the dielectric constant of the material and the moisture content. Therefore the actual dielectric–moisture content relationship is dependent on the drying and wetting history of the deposit.

[48] Finally, here we have assumed that the transmitted waveform and receiver response does not change as the antenna traverses the borehole. In reality both antennas will couple differently to materials of different EM properties, which will effect the radiation pattern of the sensors, and thus the nature of the measured waveform. Ultimately this could lead to errors in the travel time estimates. Determining how much influence these, and other more subtle phenomena have on GPR-derived moisture contents, and how these phenomena influence the error in GPR measurements, provide ample opportunities for future research.

[49] **Acknowledgments.** This work was performed at the Sandia National Laboratories, the University of Wisconsin, and the New Mexico Institute of Mines and Technology, with funding provided by the U.S. Department of Energy's Environmental Management Science Program under contract DE-AC04-94AL85000.

References

Aldridge, D. F., and D. W. Oldenburg, Two-dimensional tomographic inversion with finite-difference travel times, *J. Seism. Explor.*, *2*, 257–274, 1993.

Binley, A., P. Winship, R. Middleton, M. Pokar, and J. West, High-resolution characterization of vadose zone dynamics using cross-borehole radar, *Water Resour. Res.*, *37*, 2639–2652, 2001.

Brainard, J. R., R. J. Glass, D. L. Alumbaugh, L. Paprocki, D. J. Labrecque, X. Yang, T.-C. J. Yeh, K. E. Baker, and C. A. Rautman, The Sandia-Tech vadose zone facility: Experimental design and data report of a constant

flux infiltration experiment, Sandia Rep. SAND02-2168, Sandia Natl. Lab., Albuquerque, N. M., 2002.

Bregman, N. D., R. C. Bailey, and C. H. Chapman, Crosshole seismic tomography, *Geophysics*, *54*(2), 200–215, 1989.

Chan, C. Y., and R. J. Knight, Determining water content and saturation from dielectric measurements in layered materials, *Water Resour. Res.*, *35*, 85–93, 1999.

Dirksen, C., and S. Dasberg, Improved calibration of time domain reflectometry soil water content measurements, *Soil Sci. Soc. Am. J.*, *57*, 660–667, 1993.

Eppstein, M. J., and D. E. Dougherty, Efficient three-dimensional data inversion: Soil characterization and moisture monitoring from cross-well ground-penetrating radar at a Vermont test site, *Water Resour. Res.*, *34*, 1889–1900, 1998.

Greaves, R. J., D. P. Lesmes, J. M. Lee, and M. N. Toksoz, Velocity variations and water content estimated from multi-offset, ground-penetrating radar, *Geophysics*, *61*(3), 683–695, 1996.

Hawley, H. W., Geomorphic evolution of Socorro area of Rio Grande Valley, New Mexico Geol. Soc. Guidebook, 34th Field Conf., Socorro Reg. II, p. 334, 1983.

Hubbard, S. S., Y. Rubin, and E. Majer, Ground-penetrating-radar-assisted saturation and permeability estimation in bimodal systems, *Water Resour. Res.*, *33*, 971–990, 1997a.

Hubbard, S. S., J. E. Peterson, E. L. Majer, P. T. Zawislanski, K. H. Williams, J. Roberts, and F. Wobber, Estimation of permeable pathways and water content using tomographic radar data, *Leading Edge*, *16*, 1623–1628, 1997b.

Hughson, D. L., and T.-C. J. Yeh, A geostatistically based inverse model for three-dimensional variably saturated flow, *Stochastic Hydrol. Hydraul.*, *12*, 285–298, 1998.

Jacobsen, O. H., and P. Schjønning, A laboratory calibration of time domain reflectometry for soil water measurement including effects of bulk density and texture, *J. Hydrol.*, *151*, 147–157, 1993a.

Jacobsen, O. H., and P. Schjønning, Field evaluation of time domain reflectometry for soil water measurements, *J. Hydrol.*, *151*, 159–172, 1993b.

Kak, A. A., and M. S. Slaney, *Principles of Computerized Tomographic Imaging*, IEEE Press, Piscataway, N. J., 1988.

Knight, R. J., and A. Nur, Geometrical effects in the dielectric response of partially saturated sandstones, *Log Anal.*, *5*, 513–519, 1983.

Lesmes, D. P., R. J. Herbstzuber, and D. Wertz, Terrain Permittivity Mapping: GPR measurements of near-surface soil moisture, in *Proceedings of the Symposium on the Application of Geophysics for Environmental and Engineering Problems (SAGEEP) '99*, pp. 575–582, Environ. and Eng. Geophys. Soc., Englewood, Colo., 1999.

Paprocki, L. T., Characterization of vadose zone in-situ moisture content and an advancing wetting front using cross borehole ground penetrating radar, Masters thesis, New Mexico Inst. of Min. and Technol., Socorro, N. M., 2000.

Peterson, J. E., Pre-inversion correction and analysis of radar tomographic data, *J. Environ. Eng. Geophys.*, *6*, 1–18, 2001.

Peterson, J. E., E. L. Majer, and M. D. Knoll, Hydrological property estimation using tomographic data at the Boise Hydrogeophysical Research Sit, in *Proceedings of the Symposium on the Application of Geophysics for Environmental and Engineering Problems (SAGEEP) '99*, pp. 629–638, 1999.

Reynolds, J. M., *An Introduction to Applied and Environmental Geophysics*, John Wiley, New York, 1998.

Robinson, D. A., J. P. Bell, and C. H. Batchelor, Influence of iron minerals on the determination of soil water content using dielectric techniques, *J. Hydrol.*, *161*, 169–180, 1994.

Tarantola, A., *Inverse Problem Theory*, Elsevier Sci., New York, 1987.

Topp, G. C., J. L. Davis, and A. P. Annan, Electromagnetic determination of soil water content: Measurements in coaxial transmission lines, *Water Resour. Res.*, *16*, 574–582, 1980.

Vidale, J., Finite-difference calculation of travel times, *BSSA*, *78*, 2062–2076, 1988.

Wang, T., and A. C. Tripp, FDTD simulation of EM wave propagation in 3-D media, *Geophysics*, *61*(1), 110–120, 1997.

Wilson, L. G., L. G. Everett, and S. J. Cullen, *Handbook of Vadose Zone Characterization and Monitoring*, CRC Press, Boca Raton, Fla., 1995.

Young, M. H., J. B. Fleming, P. J. Wierenga, and A. W. Warrick, Rapid laboratory calibration of time domain reflectometry using upward infiltration, *Soil Sci. Soc. Am. J.*, *61*, 707–712, 1997.

Zegelin, S. J., I. White, and G. F. Russell, A critique of the time domain reflectometry technique for determining field soil–water content, in *Advances in Measurement of Soil Physical Properties: Bringing Theory into Practice, Soil Sci. Soc. Am. Spec. Publ.*, vol. 30, pp. 187–208, Soil Sci. Soc. of Am., Madison, Wisc., 1992.

D. Alumbaugh and P. Y. Chang, Geological Engineering Program, University of Wisconsin-Madison, 2258 Engineering Hall, 1415 Engineering Drive, Madison, WI 53706, USA. (alumbaug@engr.wisc.edu)

J. R. Brainard, R. J. Glass, and C. A. Rautman, Sandia National Laboratories, Albuquerque, NM, USA.

L. Paprocki, Komex, 5455 Garden Grove Boulevard, 2nd floor, Westminster, CA 92683, USA.